Advances in Applied Mathematics and Mechanics
Adv. Appl. Math. Mech., Vol. **5**, No. 1, pp. 90-112

DOI: 10.4208/aamm.11-m11182
February 2013

Free Vibration Analysis of Nanocomposite Plates Reinforced by Graded Carbon Nanotubes Based on First-Order Shear Deformation Plate Theory

S. Jafari Mehrabadi[1,*], B. Sobhaniaragh[2] and V. Pourdonya[1]

[1] *Department of Mechanical Engineering, Arak Branch, Islamic Azad University, Arak, Iran*
[2] *Young Researchers Club, Arak Branch, Islamic Azad University, Arak, Iran*

Received 30 November 2011; Accepted (in revised version) 6 October 2012

Available online 25 January 2013

Abstract. Based on the Mindlin's first-order shear deformation plate theory this paper focuses on the free vibration behavior of functionally graded nanocomposite plates reinforced by aligned and straight single-walled carbon nanotubes (SWCNTs). The material properties of simply supported functionally graded carbon nanotube-reinforced (FGCNTR) plates are assumed to be graded in the thickness direction. The effective material properties at a point are estimated by either the Eshelby-Mori-Tanaka approach or the extended rule of mixture. Two types of symmetric carbon nanotubes (CNTs) volume fraction profiles are presented in this paper. The equations of motion and related boundary conditions are derived using the Hamilton's principle. A semi-analytical solution composed of generalized differential quadrature (GDQ) method, as an efficient and accurate numerical method, and series solution is adopted to solve the equations of motions. The primary contribution of the present work is to provide a comparative study of the natural frequencies obtained by extended rule of mixture and Eshelby-Mori-Tanaka method. The detailed parametric studies are carried out to study the influences various types of the CNTs volume fraction profiles, geometrical parameters and CNTs volume fraction on the free vibration characteristics of FGCNTR plates. The results reveal that the prediction methods of effective material properties have an insignificant influence of the variation of the frequency parameters with the plate aspect ratio and the CNTs volume fraction.

AMS subject classifications: 35G05, 37N15, 74S30

Key words: Carbon nanotube-reinforced, functionally graded, Hamilton's principle, Eshelby-Mori-Tanaka, symmetric profiles, extended rule of mixture.

*Corresponding author.
Email: s-jafari@iau-arak.ac.ir (S. Jafari Mehrabadi)

1 Introduction

In recent years, nanotechnology has sparked a major breakthrough in materials science leading to the next industrial revolution to begin. Nanostructured materials such as graphene sheets (GSs), fullerenes and carbon nanotubes (CNTs) are fundamental building blocks of nanotechnology with wide potential applications in the emerging field of nanoelectromechanical systems. Carbon nanotubes (CNTs) have attracted much attention because of their superior mechanical, optical, thermal and electrical properties and potential applications of novel nanostructures [1–3]. Further development of CNT-based devices requires a good understanding of their mechanical behavior. Basic mechanical properties such as Young's modulus, shear modulus, Poisson's ratio and maximum tensile and compressive strengths have been studied rigorously, a review of which is given by Qian et al. [4]. Polymer composites consisting of polymers reinforced with various additives such as carbon fibers, graphite fibers, glass fibers, or Kevlar fibers and carbon black are increasingly being used in defense, aerospace, automobile, sports and electronics sectors as light-weight, high strength and high electrical and thermal conducting materials [5–8]. However, the addition of nano-sized fibers or nanofillers, such as CNTs, can further increase the merits of such composite materials. These nanocomposites, easily processed due to the small diameter of the carbon nanotubes (CNTs), exhibit unique properties [9, 10], such as enhanced modulus and tensile strength, high thermal stability and good environmental resistance. This behavior, combined with their low density makes them suitable for a broad range of technological sectors such as telecommunications, electronics [11] and transport industries, especially for aeronautic and aerospace applications where the reduction of weight is crucial in order to reduce the fuel consumption. For example, Qian et al. [12] showed that the addition of 1wt.% (i.e., 1% by weight) multiwall carbon nanotube to polystyrene resulted in 36-42% and $\sim$25% increases in the elastic modulus and the break stress of the nanocomposite properties, respectively.

Motivated by the concept of functionally graded materials (FGMs), Shen [13] suggested that for CNT-reinforced composite structures the distributions of CNTs within an isotropic matrix were designed purposefully to grade with certain rules along desired directions for the improvement of the mechanical properties of the structures and the nonlinear bending behaviors of the resulting functionally graded CNT reinforced composite (FG-CNTRC) plates in thermal environments were presented. With the knowledge that load transfer between the nanotube and polymeric phases is less than perfect (e.g., the surface effects, strain gradients effects, intermolecular coupled stress effects, etc), Shen introduced the CNT efficiency parameters to account load transfer between the nanotube and polymeric phases and other effects on the material properties of CNTRCs. They determined CNT efficiency parameters by matching the elastic modulus of CNTRCs observed from the MD simulation results with the numerical results obtained from the extended rule of mixture. Wang and Shen [14] investigated the large amplitude vibration of nanocomposite sandwich plates reinforced by SWCNTs resting on an elastic foundation in thermal environments. The effect of CNT volume fraction on the com-

pressive postbuckling and thermal postbuckling behavior of functionally graded CNTRC plates was reported by Shen and Zhu [15] and Shen and Zhang [16]. They found that in some cases the CNTRC plate with intermediate CNT volume fraction does not have intermediate buckling temperature and initial thermal postbuckling strength. Ke et al. [17] investigated the nonlinear free vibration of functionally graded CNTRC Timoshenko beams. They found that both linear and nonlinear frequencies of functionally graded CNTRC beam with symmetrical distribution of CNTs are higher than those of beams with uniform or unsymmetrical distribution of CNTs. Yas and Heshmati [18] investigated vibrational characteristics of functionally graded nanocomposite beams reinforced by randomly oriented straight SWCNTs under the action of moving load. They used the Eshelby-Mori-Tanaka approach based on an equivalent fiber to investigate the material properties of the beam and also they used finite element method to discretize the model and obtain a numerical approximation of the motion equation. Moradi-Dastjerdi et al. [19] studied dynamic analysis of nanocomposite cylinders reinforced by single-walled carbon nanotubes subjected to an impact load was carried out by a mesh-free method. An axisymmetric model was used and volume fraction of CNT was assumed to vary continuously along thickness direction. The effective material properties of functionally graded carbon nanotube were estimated using extended rule of mixture. Very recently, bending behavior of functionally graded carbon nanotube reinforced composite plate embedded in thin piezoelectric layers subjected to mechanical uniform load based on three-dimensional theory of elasticity was studied by Alibeigloo [20].

The main aim of this paper is to present free vibration analysis of the functionally graded carbon nanotube-reinforced (FGCNTR) plates by making the use of the first-order shear deformation theory (FSDT) and generalized differential quadrature (GDQ) method. The FGCNTR plate is assumed to be made from a mixture of aligned and straight SWCNT, graded distribution in the thickness direction, and matrix which is assumed to be isotropic. This paper deals with harmonic oscillation of CNT-reinforced plates, which presumes that the deflection amplitude is much smaller than the thickness of a plate. The material properties of SWCNT are determined according to molecular dynamics (MD) and then the effective material properties of CNTRCs are estimated through the rule of mixture in which the CNT efficiency parameters are introduced to account for the scale-dependence of the resulting nanostructures. Furthermore, the material properties of SWCNT can be used to calculate the elastic properties of nanocomposites using the Mori-Tanaka modified approach that utilizes Eshelby tensors. The primary contribution of the present work is to provide a comparative study of the natural frequencies obtained by extended rule of mixture and Eshelby-Mori-Tanaka method. Two types of the symmetric carbon nanotubes (CNTs) volume fraction profiles are presented in this paper. The effects of various types of the CNTs volume fraction profiles, geometrical parameters and CNT s volume fraction on the free vibration characteristics of FGCNTR plates are discussed in detail. The results for CNTRC plates with uniformly distributed CNTs are also provided for comparison. The results of the parametric studies show that the above mention effects play very important role on the free vibration behavior of the

FGCNTR plates and it is believed that interesting and new results are presented for free vibration characteristics of FGM nano-structure plates which are of interest to the scientific and engineering community in the area of nano-structures.

2 Problem formulation

2.1 Geometrical configuration

A flat, nanocomposite rectangular plate of length a, width b and uniform thickness h, made of functionally graded materials carbon nanotube-recinforced is depicted in Fig. 1. The Cartesian coordinate system (x,y,z) is considered to extract mathematical formulations when x and y axes are located in the undeformed midplane of the plate.

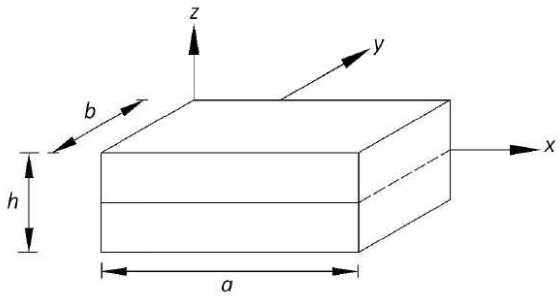

Figure 1: Configuration of an FGCNTR rectangular plate.

2.2 Material properties of FGCNTR

We assume that the FGCNTR plate is made from a mixture of aligned and straight SWCNT, graded distribution in the thickness direction, and matrix which is assumed to be isotropic. In this paper, for the first time, two types of symmetric profiles for CNTs volume fractions are configurated. As can be seen from Fig. 2, for the first type, a mid-plane symmetric graded distribution of CNT reinforcements is achieved and both top and bottom surfaces are CNT-rich referred to as Type I FGCNTR. For the second type, the distribution of CNT reinforcements is inversed and both top and bottom surfaces are CNT-poor, whereas the mid-plane surface is CNT-rich, referred to as Type II FGCNTR. We assume the CNTs volume fraction for Type I FGCNTR follows as:

$$V_{CN}=\frac{4|z|}{h}V_{CN}^{*}, \tag{2.1}$$

in which

$$V_{CN}^{*}=\frac{w_{CN}}{w_{CN}+(\rho_{CN}/\rho_m)-(\rho_{CN}/\rho_m)w_{CN}}.$$

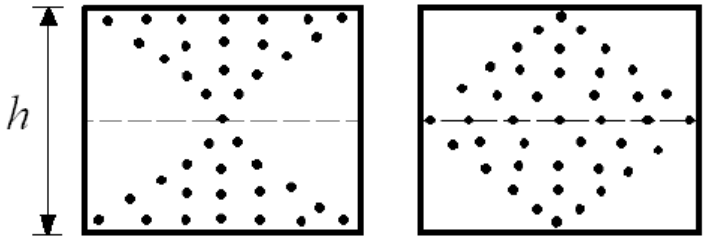

Figure 2: Configurations of FGCNTR ((a): Type I FGCNTR, (b): Type II FGCNTR).

Where w_{CN} is the mass fraction of nanotube [13, 14] and ρ_{CN} and ρ_m are the densities of CNT and matrix, respectively. The CNTs volume fraction for Type II FGCNTR follows as:

$$V_{CN} = 4\left(0.5 - \frac{|z|}{h}\right) {V_{CN}}^*. \tag{2.2}$$

Note that $V_{CN} = V_{CN}^*$ corresponds to the uniformly distributed CNTR plate, referred to as UDCNTR. It should be mentioned that these two FGCNTR plates and the UDCNTR plate have the same CNT mass fraction. The Poisson's ratio is assumed to be uniformly distributed [14, 15]:

$$v_{12} = V_{CN}^* {v_{12}}^{CN} + V_m v^m, \tag{2.3}$$

where ${v_{12}}^{CN}$ and v^m are Poisson's ratios of CNT and matrix, respectively. For the implementation of CNTRCs in structural applications, property-microstructure relations are required in the form of micromechanics models.

2.2.1 Extended rule of mixture

According to the extended rule of mixture, the effective Young's modulus and shear modulus of FGCNTR are expressed by the following relations [13–17]:

$$E_{11} = \eta_1 V_{CN} E_{11}^{CN} + V_m E^m, \quad \frac{\eta_2}{E_{22}} = \frac{V_{CN}}{E_{22}^{CN}} + \frac{V_m}{E^m}, \quad \frac{\eta_3}{G_{12}} = \frac{V_{CN}}{G_{12}^{CN}} + \frac{V_m}{G^m}, \tag{2.4}$$

where E_{11}^{CN}, E_{22}^{CN} and G_{12}^{CN} are the Young's and shear moduli of the CNTs, E^m and G^m are the corresponding properties for the matrix, and the η_i $(i = 1,2,3)$ are the CNT efficiency parameters, respectively. With the knowledge that load transfer between the nanotube and polymeric phases is less than perfect (e.g., the surface effects, strain gradients effects, intermolecular coupled stress effects, etc), Shen et al. [13] introduced the CNT efficiency parameters to account load transfer between the nanotube and polymeric phases and other effects on the material properties of CNTRCs. They determined CNT efficiency parameters by matching the elastic modulus of CNTRCs observed from the MD simulation

results with the numerical results obtained from the extended rule of mixture. V_{CN} and V_m are the carbon nanotube and matrix volume fractions and are related by:

$$V_{CN}+V_m=1. \tag{2.5}$$

2.2.2 Eshelby-Mori-Tanaka approach

The material properties of SWCNT obtained by molecular dynamics (MD) can be used to calculate the elastic properties of nanocomposites using the Mori-Tanaka modified approach that utilizes Eshelby tensors. Previous studies have examined the validity of the Eshelby-Mori-Tanaka approach in determining the effective properties of composites reinforced with misaligned, carbon fibres, and with carbon nanotubes [21–24]. For instance, Odegard et al. [21] developed constitutive models for SWNT-reinforced polymer composite materials based on the equivalent continuum modeling technique for nano-structured materials. It was proposed that the nanotube, the local polymer near the nanotube, and the nanotube/polymer interface can be modeled as an effective continuum fiber by using an equivalent-continuum modeling method. They employed the Eshelby-Mori-Tanaka approach to determine the bulk constitutive properties of the SWNT/polymer composite with aligned and random nanotube orientations and with various nanotube lengths and volume fractions. In addition, predicted values of modulus were compared with experimental data obtained from mechanical testing. As another example, Shady and Gowayed [24] modified the effective fiber model used to calculate the elastic properties of nanocomposites in order to include the effect of the curvature of nanotubes. They used the effective fiber model to calculate the elastic properties of nanocomposites using the Eshelby-Mori-Tanaka. In the present paper, the proposed model is framed within the Eshelby theory for elastic inclusions. The original theory of Eshelby [25–27] is restricted to one single inclusion in a semi-infinite elastic, homogeneous and isotropic medium. The theory, generalized by Mori-Tanaka [28], allows extending the original approach to the practical case of multiple inhomogeneities embedded into a finite domain. The Eshelby-Mori-Tanaka approach, based on the equivalent elastic inclusion idea of Eshelby and the concept of average stress in the matrix due to Mori-Tanaka, is also known as the equivalent inclusion-average stress method [29, 30]. According to Benveniste's revision [31], the following expression of the effective elastic tensor is obtained:

$$\mathbf{C}=\mathbf{C}_m+V_{CN}\langle(\mathbf{C}_f-\mathbf{C}_m)\cdot\mathbf{A}\rangle\cdot\left[V_m\mathbf{I}+V_{CN}\langle\mathbf{A}\rangle\right]^{-1}, \tag{2.6}$$

where V_{CN} and V_m are the fiber and matrix volume fractions, respectively, $\mathbf{I}$ represents the fourth-order unit tensor, $\mathbf{C}_m$ is the stiffness tensor of the matrix material, $\mathbf{C}_f$ is the stiffness tensor of the equivalent fiber, the brackets denote an average overall possible orientations of the inclusions. It should be noted that $(\cdot)$ denotes the dot product. $\mathbf{A}$ is the fourth-order tensor referred to as concentration factor:

$$\mathbf{A}=\left[\mathbf{I}+\mathbf{S}\cdot{\mathbf{C}_m}^{-1}\cdot\left(\mathbf{C}_f-\mathbf{C}_m\right)\right]^{-1}. \tag{2.7}$$

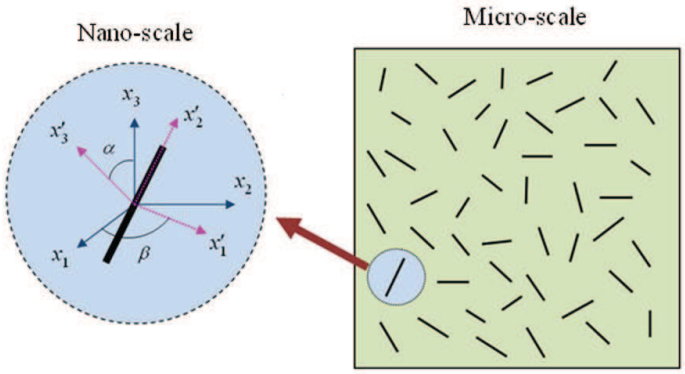

Figure 3: Representative volume element (RVE) including straight CNTs.

The tensor **S** is Eshelby's tensor, as given by Eshelby [25] and Mura [31]. The terms included in angle brackets in Eq. (2.6) represent the average value of the term over all orientations defined by transformation from the local fiber coordinates $(o-x'_1x'_2x'_3)$ to the global coordinates $(o-x_1x_2x_3)$ (Fig. 3).

In this paper, we consider a polymer composite reinforced with straight CNTs aligned in the x_2-axis direction. The matrix is assumed to be elastic and isotropic, with Young's modulus E_m and Poisson's ratio ν_m [29,30]. Each straight CNT is modeled as a fiber with transversely isotropic elastic properties. Therefore, the composite is also transversely isotropic. The substitution of non-vanishing components of the Eshelby tensor S for a straight, long fiber along the x_2-direction [30] in Eq. (2.7) gives the dilute mechanical strain concentration tensor. Then the substitution of A (Eq. (2.7)) into Eq. (2.6) gives the tensor of effective elastic moduli of the composite reinforced by aligned, straight CNTs. In particular, the Hill's elastic moduli are found as:

$$k=\frac{E_m\{E_mV_m+2k_r(1+\nu_m)[1+V_{CN}(1-2\nu_m)]\}}{2(1+\nu_m)[E_m(1+V_{CN}-2\nu_m)+2V_mk_r(1-\nu_m-2\nu_m^2)]}, \tag{2.8a}$$

$$l=\frac{E_m\{\nu_mV_m[E_m+2k_r(1+\nu_m)]+2V_{CN}{}_rk_r(1-\nu_m^2)\}}{(1+\nu_m)[E_m(1+V_{CN}-2\nu_m)+2V_mk_r(1-\nu_m-2\nu_m^2)]}, \tag{2.8b}$$

$$\begin{aligned}n=&\frac{E_m^2V_m(1+V_{CN}-V_m\nu_m)+2V_mV_{CN}(k_rn_r-l_r^2)(1+\nu_m)^2(1-2\nu_m)}{(1+\nu_m)[E_m(1+V_{CN}-2\nu_m)+2V_mk_r(1-\nu_m-2\nu_m^2)]}\\&+\frac{E_m[2V_m^2k_r(1-\nu_m)+V_{CN}n_r(1+V_{CN}-2\nu_m)-4V_ml_r\nu_m]}{E_m(1+V_{CN}-2\nu_m)+2V_mk_r(1-\nu_m-2\nu_m^2)},\end{aligned} \tag{2.8c}$$

$$p=\frac{E_m[E_mV_m+2p_r(1+\nu_m)(1+V_{CN})]}{2(1+\nu_m)[E_m(1+V_{CN})+2V_mp_r(1+\nu_m)]}, \tag{2.8d}$$

$$\xi=\frac{E_m[E_mV_m+2m_r(1+\nu_m)(3+V_{CN}-4\nu_m)]}{2(1+\nu_m)\{E_m[V_m+4V_{CN}(1-\nu_m)]+2V_mm_r(3-\nu_m-4\nu_m^2)\}}, \tag{2.8e}$$

where ξ, l, m, n and p are Hill's elastic moduli of the composite; ξ is the plane-strain

bulk modulus normal to the fiber direction, n is the uniaxial tension modulus in the fiber direction, l is the associated cross modulus, m and p are the shear moduli in planes normal and parallel to the fiber direction, respectively. k_r, l_r, m_r, n_r and p_r are the Hill's elastic moduli for the reinforcing phase (CNTs) [32]. The elastic moduli parallel and normal to CNTs are related to Hill's elastic moduli by

$$E_L = n - \frac{l^2}{\xi}, \quad E_T = \frac{4m(\xi n - l^2)}{\xi n - l^2 + mn}, \quad G_{LT} = 2p, \quad v_{LT} = \frac{l}{2\xi}. \tag{2.9}$$

2.3 Constitutive relations

According to the based on the first-order shear deformation theory of Mindlin [33–35], in which the in-plane displacements are expanded as linear functions of the thickness coordinate and the transverse deflection is constant through the plate thickness, the displacement components of the middle surface of the rectangular plate along the x, y, and z axes, designated by u, v and w, may be expressed as:

$$u(x,y,z,t) = u_0(x,y,t) + z\varphi_x(x,y,t), \tag{2.10a}$$
$$v(x,y,z,t) = v_0(x,y,t) + z\varphi_y(x,y,t), \tag{2.10b}$$
$$w(x,y,z,t) = w_0(x,y,t), \tag{2.10c}$$

where u_0 and v_0 denote the in-plane displacements on mid-plane in x- and y- directions, respectively; w_0 is the transverse displacement; φ_x and φ_y are the rotational displacements about the x and y axes at the middle surface of the plate and t is the time.

By neglecting normal strain in the thickness direction ε_{zz} in the stress-strain relations, the general strain-displacement relations for small deformation are defined as:

$$\varepsilon_{xx} = u_{,x}, \quad \varepsilon_{yy} = v_{,y}, \quad \gamma_{xy} = u_{,y} + v_{,x}, \quad \gamma_{yz} = v_{,z} + w_{,y}, \quad \gamma_{xz} = u_{,z} + w_{,x}, \tag{2.11}$$

where ε and γ denote the normal and shear strains, respectively. Here, the symbol "," is used to indicate the partial derivative. For example, $v_{,y}$ is equivalent to $\partial v/\partial y$. By substituting the Eq. (2.10) into Eq. (2.11), the strain-displacement relations are derived:

$$\{\varepsilon_{ij}\} = \{\varepsilon^0{}_{ij}\} + z\{\varepsilon^1{}_{ij}\}, \quad i,j = x,y,z, \tag{2.12}$$

where

$$\begin{Bmatrix} \varepsilon^0_{xx} \\ \varepsilon^0_{yy} \\ \gamma^0_{yz} \\ \gamma^0_{xz} \\ \gamma^0_{xy} \end{Bmatrix} = \begin{Bmatrix} u_{0,x} \\ v_{0,y} \\ w_{0,y} + \varphi_y \\ w_{0,x} + \varphi_x \\ u_{0,y} + v_{0,x} \end{Bmatrix}, \qquad \begin{Bmatrix} \varepsilon^1_{xx} \\ \varepsilon^1_{yy} \\ \gamma^1_{yz} \\ \gamma^1_{xz} \\ \gamma^1_{xy} \end{Bmatrix} = \begin{Bmatrix} \varphi_{x,x} \\ \varphi_{y,y} \\ 0 \\ 0 \\ \varphi_{x,y} + \varphi_{y,x} \end{Bmatrix}. \tag{2.13}$$

The constitutive relation for an FGCNTR plate is consequently given by the two-dimensional Hooke's law as:

$$\begin{Bmatrix} \sigma_{xx} \\ \sigma_{yy} \\ \tau_{yz} \\ \tau_{xz} \\ \tau_{xy} \end{Bmatrix} = \begin{bmatrix} Q_{11} & Q_{12} & 0 & 0 & 0 \\ Q_{12} & Q_{22} & 0 & 0 & 0 \\ 0 & 0 & Q_{44} & 0 & 0 \\ 0 & 0 & 0 & Q_{55} & 0 \\ 0 & 0 & 0 & 0 & Q_{66} \end{bmatrix} \begin{Bmatrix} \varepsilon_{xx} \\ \varepsilon_{yy} \\ \gamma_{yz} \\ \gamma_{xz} \\ \gamma_{xy} \end{Bmatrix}. \tag{2.14}$$

In which the Q_{ij} components are expressed as:

$$Q_{11} = \frac{E_{11}}{1-{v_{12}}^2}, \qquad Q_{12} = \frac{vE_{22}}{1-{v_{12}}^2} = \frac{vE_{11}}{1-{v_{12}}^2}, \qquad Q_{22} = \frac{E_{22}}{1-{v_{12}}^2}, \tag{2.15a}$$

$$Q_{55} = G_{13}, \qquad Q_{44} = G_{23}, \qquad Q_{66} = G_{12}, \tag{2.15b}$$

where E_{ii}, G_{ij} and v are Young's modulus, shear moduli and Poisson's ratio of the FGCNTR plate, respectively. The stress resultant-displacement relations are given by:

$$(N_i, M_i) = \int_{-\frac{h}{2}}^{\frac{h}{2}} \sigma_i(1,z)dz, \qquad i = xx, yy, xy, \tag{2.16a}$$

$$Q_i = k\int_{-\frac{h}{2}}^{\frac{h}{2}} \sigma_{iz}dz, \qquad i = x, y, \tag{2.16b}$$

in which k is the transverse shear correction coefficient, applied to the transverse shear forces due to the fact that the transverse shear strains (γ_{xz} and γ_{yz}) have a nearly parabolic dependency to the thickness coordinate and in this study is taken as $k = 5/6$. Substituting Eqs. (2.12) and (2.13) into Eq. (2.14) and then into Eqs. (2.16a) and (2.16b) gives the forces and the resultant moments (N_{ij} and M_{ij}) and the transverse shear forces (Q_i) per unit length as follows:

$$N_{xx} = \frac{1}{1-{\nu_{12}}^2}\left[(E_{1a}+E_{1d})(\varepsilon^0_{xx}+\nu_{21}\varepsilon^0_{yy}) + (E_{1b}+E_{1e})(\varepsilon^1_{xx}+\nu_{12}\varepsilon^1_{yy})\right], \tag{2.17a}$$

$$N_{yy} = \frac{1}{1-{\nu_{12}}^2}\left[(E_{2a}+E_{2d})(\varepsilon^0_{yy}+\nu_{12}\varepsilon^0_{xx}) + (E_{2b}+E_{2e})(\varepsilon^1_{yy}+\nu_{12}\varepsilon^1_{xx})\right], \tag{2.17b}$$

$$N_{xy} = (G_{12a}+G_{12d})\gamma^0_{xy} + (G_{12b}+G_{12e})\gamma^1_{xy}, \tag{2.17c}$$

$$M_{xx} = \frac{1}{1-{\nu_{12}}^2}\left[(E_{1b}+E_{1e})(\varepsilon^0_{xx}+\nu_{12}\varepsilon^0_{yy}) + (E_{1c}+E_{1f})(\varepsilon^1_{xx}+\nu_{12}\varepsilon^1_{yy})\right], \tag{2.17d}$$

$$M_{yy} = \frac{1}{1-{\nu_{12}}^2}\left[(E_{2b}+E_{2e})(\varepsilon^0_{yy}+\nu_{12}\varepsilon^0_{xx}) + (E_{2c}+E_{2f})(\varepsilon^1_{yy}+\nu_{12}\varepsilon^1_{xx})\right], \tag{2.17e}$$

$$M_{xy} = (G_{12b}+G_{12e})\gamma^0_{xy} + (G_{12c}+G_{12f})\gamma^1_{xy}, \tag{2.17f}$$

$$Q_x = k(G_{12a}+G_{12d})\gamma^0_{xz}, \qquad Q_y = k(G_{12a}+G_{12d})\gamma^0_{yz}, \tag{2.17g}$$

where coefficients E_{ij}, G_{12i} are as follows:

$$(E_{1a},E_{1b},E_{1c})=\int_{-\frac{h}{2}}^{0}E_{11}(1,z,z^2)dz, \qquad (E_{1d},E_{1e},E_{1f})=\int_{0}^{\frac{h}{2}}E_{11}(1,z,z^2)dz, \tag{2.18a}$$

$$(E_{2a},E_{2b},E_{2c})=\int_{-\frac{h}{2}}^{0}E_{22}(1,z,z^2)dz, \qquad (E_{2d},E_{2e},E_{2f})=\int_{0}^{\frac{h}{2}}E_{22}(1,z,z^2)dz, \tag{2.18b}$$

$$(G_{12a},G_{12b},G_{12c})=\int_{-\frac{h}{2}}^{0}G_{12}(1,z,z^2)dz, \quad (G_{12d},G_{12e},G_{12f})=\int_{0}^{\frac{h}{2}}G_{12}(1,z,z^2)dz. \tag{2.18c}$$

2.4 Equations of motion

Herein, Hamilton's principle is used to derive equations of motion based on the FSDT. The principle can be stated as follows:

$$\int_{t_1}^{t_2}(\delta K_e-\delta P_e)dt=0, \tag{2.19}$$

where

$$\begin{aligned}\delta K_e=\int_{\Omega_0}\Big\{\int_{-\frac{h}{2}}^{\frac{h}{2}}&\rho[(\dot{u}_0+z\dot{\varphi}_x)(\delta\dot{u}_0+z\delta\dot{\varphi}_x)+(\dot{v}_0+z\dot{\varphi}_y)(\delta\dot{v}_0+z\delta\dot{\varphi}_y)\\&+\dot{w}_0\delta\dot{w}_0]dz\Big\}dxdy,\end{aligned} \tag{2.20a}$$

$$\begin{aligned}\delta P_e=\int_{\Omega_0}\Big\{\int_{-\frac{h}{2}}^{\frac{h}{2}}&\big[\sigma_{xx}(\delta\varepsilon_{xx}^{(0)}+z\delta\varepsilon_{xx}^{(1)})+\sigma_{yy}(\delta\varepsilon_{yy}^{(0)}+z\delta\varepsilon_{yy}^{(1)})+\sigma_{xy}(\delta\gamma_{xy}^{(0)}+z\delta\gamma_{xy}^{(1)})\\&+\sigma_{xz}\delta\gamma_{xz}^{(0)}+\sigma_{yz}\delta\gamma_{yz}^{(0)}\big]dz\Big\}dxdy,\end{aligned} \tag{2.20b}$$

where K_e is the kinetic energy of the plate and P_e is the elastic potential energy of the FGCNTR plate. Simplifying Eqs. (2.20a) and (2.20b) and inserting the results into Eq. (2.19) and performing the integrations by parts in Hamilton's equation (2.19), one obtains

$$N_{xx,x}+N_{xy,y}=I_0\ddot{u}_0+I_1\ddot{\varphi}_x, \quad N_{xy,x}+N_{yy,y}=I_0\ddot{v}_0+I_1\ddot{\varphi}_y, \quad Q_{x,x}+Q_{y,y}=I_0\ddot{w}_0, \tag{2.21a}$$

$$M_{xx,x}+M_{xy,y}-Q_x=I_1\ddot{u}_0+I_2\ddot{\varphi}_x, \quad N_{xy,x}+N_{yy,y}-Q_y=I_1\ddot{v}_0+I_2\ddot{\varphi}_y, \tag{2.21b}$$

where

$$I_i=\int_{-\frac{h}{2}}^{\frac{h}{2}}(z)^i\rho(z)dz, \quad i=0,1,2. \tag{2.22}$$

For a simply supported FGCNTR rectangular plate, the boundary conditions can be expressed on the x-constant and y-constant edges as

$$v_0=w_0=N_{xx}=M_{xx}=\varphi_y=0 \qquad \text{at } x=0,a, \tag{2.23a}$$

$$u_0=w_0=N_{yy}=M_{yy}=\varphi_x=0 \qquad \text{at } y=0,b. \tag{2.23b}$$

This paper deals with harmonic oscillation of CNT-reinforced plates, which presumes that the deflection amplitude is much smaller than the thickness of a plate. For free harmonic vibration, the Fourier expansion form of the displacement components in the x direction which satisfy the geometric boundary conditions at $y=0$, b can be written as:

$$u_0(x,y,t)=U_n(x)\sin\left(\frac{n\pi}{b}y\right)e^{-i\omega t}, \qquad v_0(x,y,t)=V_n(x)\cos\left(\frac{n\pi}{b}y\right)e^{-i\omega t}, \tag{2.24a}$$

$$w_0(x,y,t)=W_n(x)\sin\left(\frac{n\pi}{b}y\right)e^{-i\omega t}, \qquad \varphi_x(x,y,t)=X_n(x)\sin\left(\frac{n\pi}{b}y\right)e^{-i\omega t}, \tag{2.24b}$$

$$\varphi_y(x,y,t)=Y_n(x)\cos\left(\frac{n\pi}{b}y\right)e^{-i\omega t}, \tag{2.24c}$$

where n is the wave number along the y- direction, ω is the natural frequency of the vibration and i $(=\sqrt{-1})$ is the imaginary number.

3 GDQ discretized form of the equations of motion

Discretization is based on the generalized differential quadrature method (GDQ) [36–38]. According to GDQ method the rth-order partial derivative of a continuous function $f(\zeta)$ with respect to ζ at a given point ζ_i can be approximated as a linear sum of weighted function values at all of the discrete points in the domain of ζ, i.e., [36]

$$\frac{\partial^r f(\zeta_i)}{\partial\zeta^r}=\sum_{k=1}^{N}c_{ik}^{(r)}f(\zeta_k), \quad i=1,\cdots,N, \quad r=1,\cdots,N-1, \tag{3.1}$$

where N is the number of sampling points in the axial direction, $f(\zeta_k)$ represents the functional value at a sample point ζ_k and $c_{ik}^{(r)}$ are the weighting coefficients of the rth-order derivative. The weighting coefficients for the first derivative (i.e., $r=1$) are [36]

$$c_{ij}^{(1)}=\begin{cases}\dfrac{M^{(1)}(x_i)}{(x_i-x_j)M^{(1)}(x_j)}, & i\neq j,\ i,j=1,2,\cdots,N,\\ -\displaystyle\sum_{j=1,\ i\neq j}^{N}c_{ij}^{(1)}, & i=j,\ i=1,2,\cdots,N,\end{cases} \tag{3.2}$$

where

$$M(x_i)=\prod_{j=1,\ i\neq j}^{N}(x_i-x_j). \tag{3.3}$$

For higher-order derivatives

$$c_{ij}^{(1)}=\begin{cases}r\left[c_{ii}^{(r-1)}c_{ij}^{(1)}-\dfrac{c_{ij}^{(r-1)}}{(x_i-x_j)}\right], & i\neq j,\ i,j=1,2,\cdots,N,\ r=2,3,\cdots,N-1,\\ -\displaystyle\sum_{j=1,\ i\neq j}^{N}c_{ij}^{(r)}, & i=j,\ i=1,2,\cdots,N.\end{cases} \tag{3.4}$$

After substituting Eq. (2.24) into Eq. (2.21), the partial differential equations in terms of the variables x, y and t reduces to ordinary differential equations in terms of the variable x and by application GDQ discretization rule (3.1) for spatial derivatives, the discretized form of the differential equations of motion at each domain grid point x_i with $(i=2,3,\cdots,N_x-1)$ can be obtained as:

$$\begin{aligned}
&\frac{1}{1-\nu_{12}^2}\Big[(E_{1a}+E_{1d})\Big(\sum_{k=1}^{N_x}c_{ik}^{(2)}U_{nk}-\frac{n\pi}{b}\nu_{12}\sum_{k=1}^{N_x}c_{ik}^{(1)}V_{nk}\Big)+(E_{1b}+E_{1e})\Big(\sum_{k=1}^{N_x}c_{ik}^{(2)}X_{nk}\\
&\quad-\frac{n\pi}{b}\nu_{12}\sum_{k=1}^{N_x}c_{ik}^{(1)}Y_{nk}\Big)\Big]+(G_{12a}+G_{12d})\Big(-\Big(\frac{n\pi}{b}\Big)^2U_{ni}-\frac{n\pi}{b}\sum_{k=1}^{N_x}c_{ik}^{(1)}V_{nk}\Big)\\
&\quad+(G_{12b}+G_{12e})\Big(-\Big(\frac{n\pi}{b}\Big)^2X_{ni}-\frac{n\pi}{b}\sum_{k=1}^{N_x}c_{ik}^{(1)}Y_{nk}\Big)\\
&=(\rho_a+\rho_d)\omega^2U_{ni}+(\rho_b+\rho_e)\omega^2X_{ni},
\end{aligned}\tag{3.5a}$$

$$\begin{aligned}
&\frac{1}{1-\nu_{12}^2}\Big[(E_{2a}+E_{2d})\Big(-\Big(\frac{n\pi}{b}\Big)^2V_{ni}+\frac{n\pi}{b}\nu_{12}\sum_{k=1}^{N_x}c_{ik}^{(1)}U_{nk}\Big)+(E_{2b}+E_{2e})\Big(-\Big(\frac{n\pi}{b}\Big)^2Y_{ni}\\
&\quad+\frac{n\pi}{b}\nu_{12}\sum_{k=1}^{N_x}c_{ik}^{(1)}X_{nk}\Big)\Big]+(G_{12a}+G_{12d})\Big(\frac{n\pi}{b}\sum_{k=1}^{N_x}c_{ik}^{(1)}U_{nk}+\sum_{k=1}^{N_x}c_{ik}^{(2)}V_{nk}\Big)\\
&\quad+(G_{12b}+G_{12e})\Big(\frac{n\pi}{b}\sum_{k=1}^{N_x}c_{ik}^{(1)}X_{nk}+\sum_{k=1}^{N_x}c_{ik}^{(2)}Y_{nk}\Big)\\
&=(\rho_a+\rho_d)\omega^2V_{ni}+(\rho_b+\rho_e)\omega^2Y_{ni},
\end{aligned}\tag{3.5b}$$

$$\begin{aligned}
&k(G_12a+G_12d)\Big(\sum_{k=1}^{N_x}c_{ik}^{(2)}W_{nk}+\sum_{k=1}^{N_x}c_{ik}^{(1)}X_{nk}\Big)\\
&\quad+k(G_12a+G_12d)\Big(-\Big(\frac{n\pi}{b}\Big)^2W_{ni}-\Big(\frac{n\pi}{b}\Big)Y_{ni}\Big)\\
&=(\rho_a+\rho_d)\omega^2W_{ni},
\end{aligned}\tag{3.5c}$$

$$\begin{aligned}
&\frac{1}{1-\nu_{12}^2}\Big[(E_{1b}+E_{1e})\Big(\sum_{k=1}^{N_x}c_{ik}^{(2)}U_{nk}-\frac{n\pi}{b}\nu_{12}\sum_{k=1}^{N_x}c_{ik}^{(1)}V_{nk}\Big)+(E_{1c}+E_{1f})\Big(\sum_{k=1}^{N_x}c_{ik}^{(2)}X_{nk}\\
&\quad-\Big(\frac{n\pi}{b}\Big)\nu_{12}\sum_{k=1}^{N_x}c_{ik}{}^{(1)}Y_{nk}\Big)\Big]+(G_{12b}+G_{12e})\Big(-\Big(\frac{n\pi}{b}\Big)^2U_{ni}-\frac{n\pi}{b}\sum_{k=1}^{N_x}c_{ik}^{(1)}V_{nk}\Big)\\
&\quad+(G_{12c}+G_{12f})\Big(\Big(\frac{n\pi}{b}\Big)^2X_{ni}-\frac{n\pi}{b}\sum_{k=1}^{N_x}c_{ik}^{(1)}Y_{nk}\Big)-k(G_{12a}+G_{12d})\Big(\sum_{k=1}^{N_x}c_{ik}^{(1)}W_{nk}+X_{ni}\Big)\\
&=(\rho_b+\rho_e)\omega^2U_{ni}+(\rho_c+\rho_f)\omega^2X_{ni},
\end{aligned}\tag{3.5d}$$

$$\frac{1}{1-\nu_{12}{}^2}\Big[(E_{2b}+E_{2e})\Big(-\Big(\frac{n\pi}{b}\Big)^2 V_{ni}+\nu_{12}\frac{n\pi}{b}\sum_{k=1}^{N_x}c_{ik}^{(1)}U_{nk}\Big)+(E_{2c}+E_{2f})\Big(-\Big(\frac{n\pi}{b}\Big)^2 Y_{ni}$$
$$+\nu_{12}\frac{n\pi}{b}\sum_{k=1}^{N_x}c_{ik}^{(1)}X_{nk}\Big)\Big]+(G_{12b}+G_{12e})\Big(\frac{n\pi}{b}\sum_{k=1}^{N_x}c_{ik}^{(1)}U_{nk}+\sum_{k=1}^{N_x}c_{ik}^{(2)}V_{nk}\Big)$$
$$+(G_{12c}+G_{12f})\Big(\frac{n\pi}{b}\sum_{k=1}^{N_x}c_{ik}^{(1)}X_{nk}+\sum_{k=1}^{N_x}c_{ik}^{(2)}Y_{nk}\Big)-k(G_{12a}+G_{12d})\Big(-\frac{n\pi}{b}W_{ni}+Y_{ni}\Big)$$
$$=(\rho_b+\rho_e)\omega^2 V_{ni}+(\rho_c+\rho_f)\omega^2 Y_{ni}, \tag{3.5e}$$

where

$$(\rho_a,\rho_b,\rho_c)=\int_{-\frac{h}{2}}^{0}\rho(1,z,z^2)dz,\quad (\rho_d,\rho_e,\rho_f)=\int_{0}^{\frac{h}{2}}\rho(1,z,z^2)dz. \tag{3.6}$$

In Eqs. (3.5a)-(3.5e), $c_{ik}^{(1)}$ and $c_{ik}^{(2)}$ are the weighting coefficients of the first and second order derivatives. In a similar manner, at each boundary grid points, the boundary conditions (2.23a) are discretized.

Rearranging the GDQ analogs of field equations and boundary conditions within the framework of a generalized eigenvalue problem yields [40]

$$\begin{bmatrix}[K_{dd}] & [K_{db}]\\ [K_{bd}] & [K_{bb}]\end{bmatrix}\begin{Bmatrix}\delta_d\\ \delta_b\end{Bmatrix}=\begin{Bmatrix}\{\omega^2\}[M]\{\delta_d\}\\ \{0\}\end{Bmatrix}, \tag{3.7}$$

in which the subscripts b and d refer to the boundary and domain grid points, respectively. $[K_{dd}]$, $[K_{db}]$, $[K_{bd}]$ and $[K_{bb}]$ are the stiffness matrices. The matrix $[M]$ corresponds to inertia terms. The displacement vectors δ_d and δ_b are defined by:

$$\{\delta_d\}=\Big[\{\Gamma_d^{(1)}\}\quad\{\Gamma_d^{(2)}\}\quad\cdots\quad\{\Gamma_d^{(N)}\}\Big]^T,\quad \{\Gamma_d^{(i)}\}=\Big[U_d^{(i)}\quad Y_d^{(i)}\quad W_d^{(i)}\quad X_d^{(i)}\quad Y_d^{(i)}\Big]^T \tag{3.8}$$

with $i=1,2,\cdots,N_x$ and

$$\{\delta_b\}=\Big[\{\Gamma_b^{(1)}\}\quad\{\Gamma_b^{(2)}\}\quad\cdots\quad\{\Gamma_b^{(N)}\}\Big]^T,\quad \{\Gamma_b^{(i)}\}=\Big[U_b^{(i)}\quad Y_b^{(i)}\quad W_b^{(i)}\quad X_b^{(i)}\quad Y_b^{(i)}\Big]^T \tag{3.9}$$

with $i=1,2,\cdots,N_x$.

Eliminating the boundary degrees of freedom [40,41], Eq. (3.7) can be recast into the standard form of:

$$[M]^{-1}[K_{dd}]-[K_{db}][K_{bb}]^{-1}[K_{bd}]\{\delta_d\}-\omega^2[I]\{\delta_d\}=0, \tag{3.10}$$

where $[I]$ is identity matrix. The above eigenvalue system of equations can be solved to find the natural frequencies of the FGCNTR rectangular plate.

4 Numerical results and discussions

4.1 Comparison study and convergence behavior

In order to validate the presented approach and to examine its computational efficiency, its convergence and accuracy is demonstrated via different examples. As a first example to validate the presented formulations, the obtained natural frequencies of an isotropic plate based on the presented method are compared with the FSDT with and without rotary inertia by Reddy [39] in Table 1. The results are prepared for different values of the length to thickness ratio. From this table, one could observe that the present GDQ results for the isotropic square plate are in good agreement with those of FSDT with rotary inertia. The difference between without rotary inertia and present results increases as a/h is decreased. This is due to the fact that the transverse shear and rotary inertia will have more effect on a thicker plate.

As another attempt to validate the presented formulations, in Table 2 the first three non-dimensional natural frequency parameters of the FGM plate are compared with those of 3-D elasticity theory of Yas and Sobhani Aragh [40] and 2-D higher order theory of Matsunaga [41]. The fast rate of convergence of the method is evident. It should

Table 1: Comparison of the fundamental natural frequencies of an isotropic square plate.

	a/h			
	100	50	20	10
FSDT- with rotary inertia [39]	5.883	5.877	5.835	5.694
FSDT- without rotary inertia [39]	5.883	5.879	5.847	5.736
Present	5.8831	5.8770	5.8351	5.6939

Table 2: Convergence behavior and accuracy of the non-dimensional natural frequency parameters of simply supported FGM plate against the number of GDQ grid points $(b/h=2)$.

		Mode(n,l)			
p		(1,1)	(1,0)	(2,0)	(1,2)
0	$N_x=5$	0.55727	0.94006	1.5093	1.7408
	$N_x=7$	0.55723	0.94004	1.5092	1.7407
	$N_x=9$	0.55722	0.94003	1.5091	1.7406
	$N_x=13$	0.55722	0.94003	1.5091	1.7406
	3-D Elasticity [40]	0.55724	0.94004	1.5089	1.7406
	2-D higher order theory [41]	0.5572	0.94	1.509	1.7406
1	$N_x=5$	0.43759	0.74780	1.2166	1.4081
	$N_x=7$	0.43758	0.74779	1.2164	1.4077
	$N_x=9$	0.43757	0.74778	1.2162	1.4076
	$N_x=13$	0.43757	0.74778	1.2162	1.4076
	3-D Elasticity [40]	0.43739	0.74751	1.2160	1.4074
	2-D higher order theory [41]	0.4375	0.7477	1.2163	1.4078

be mentioned that only nine GDQ grid points in the x direction is sufficient to obtain results with sufficient accuracy.

4.2 Parametric studies

In this section, new numerical results for the free vibration analysis of rectangular Mindlin nanocomposite plates reinforced by single-walled CNT are presented. Poly (methyl methacrylate), referred to as PMMA, is selected for the matrix, and the material properties of which are assumed to be $\rho^m = 1.15\text{g/cm}^3$, $v^m = 0.34$, $E^m = 2.5\text{GPa}$ at room temperature (300K) [13, 14]. The $(10,10)$ SWCNTs are selected as reinforcements. The key issue for successful application of the extended rule of mixture to CNTRCs is to determine the CNT efficiency parameter η_i. There are no experiments conducted to determine the value of η_i for CNTRCs. Shen [13, 14] determined the CNT efficiency parameters η_1, η_2 and η_3 by matching the Young's moduli E_{11} and E_{22} and shear modulus G_{12} of CNTRCs predicted from the extended rule of mixture to those from the MD simulations given by Han and Elliott [42]. For example, $\eta_1 = 0.137$, $\eta_2 = 1.022$ and $\eta_3 = 0.715$ for the case of $V^*_{CN} = 0.12$ and $\eta_1 = 0.142$, $\eta_2 = 1.626$ and $\eta_3 = 1.138$ for the case of $V^*_{CN} = 0.17$ and $\eta_1 = 0.141$, $\eta_2 = 1.585$ and $\eta_3 = 1.109$ for the case of $V^*_{CN} = 0.28$. These values will be used in all the following examples, in which taking $\eta_3 : \eta_2 = 0.7 : 1$ and $G_{13} = G_{12}$ and $G_{23} = 1.2G_{12}$ [14]. In this paper, natural frequencies of the FGCNTR plate are obtained and considered to be dimensionless as $\Omega_{nl} = \omega_{nl} h \sqrt{\rho^m / E^m}$ (called the frequency parameter).

4.2.1 Effect of profiles of CNTs volume fractions on frequency parameters

Fig. 4 shows the first three frequency parameters versus thickness to length ratio h/a with different profiles of CNTs volume fractions and various types of CNT volume fraction profiles. It can be seen that the plates with Type I FGCNTR and Type II FGCNTR have highest and lowest frequency parameter, respectively. This means that the FGCNTR plates with symmetric profiles of the CNTs volume fraction can likely be designed according to the actual requirement and it is a potential alternative to the CNTRc plates with uniformly distributed CNTs. Moreover, with increasing wave number n, the discrepancies between the frequency parameters of the various types of CNTs volume fraction profiles become lower.

4.2.2 Influence of geometrical parameters on frequency parameters

Fig. 5 depicts the effect of thickness to length ratio on the fundamental frequency parameter of the FGCNTR plate for different values of b/a ratio with $V^*_{CN} = 0.12$. The results in Fig. 5 indicate that the fundamental frequency parameter increases with the increasing values of the h/a ratio. Fundamental frequency parameter ratio of the CNTRc plate for various h/a and b/a ratio is calculated and plotted in Fig. 6. It is worthy to mention that frequency parameter ratio decreases rapidly with the increase of the b/a ratio for different values of the h/a ratio and then approach a constant value for higher b/a ratio. It is interesting to note that the effect of the h/a ratio on the Type II FGCNRT to

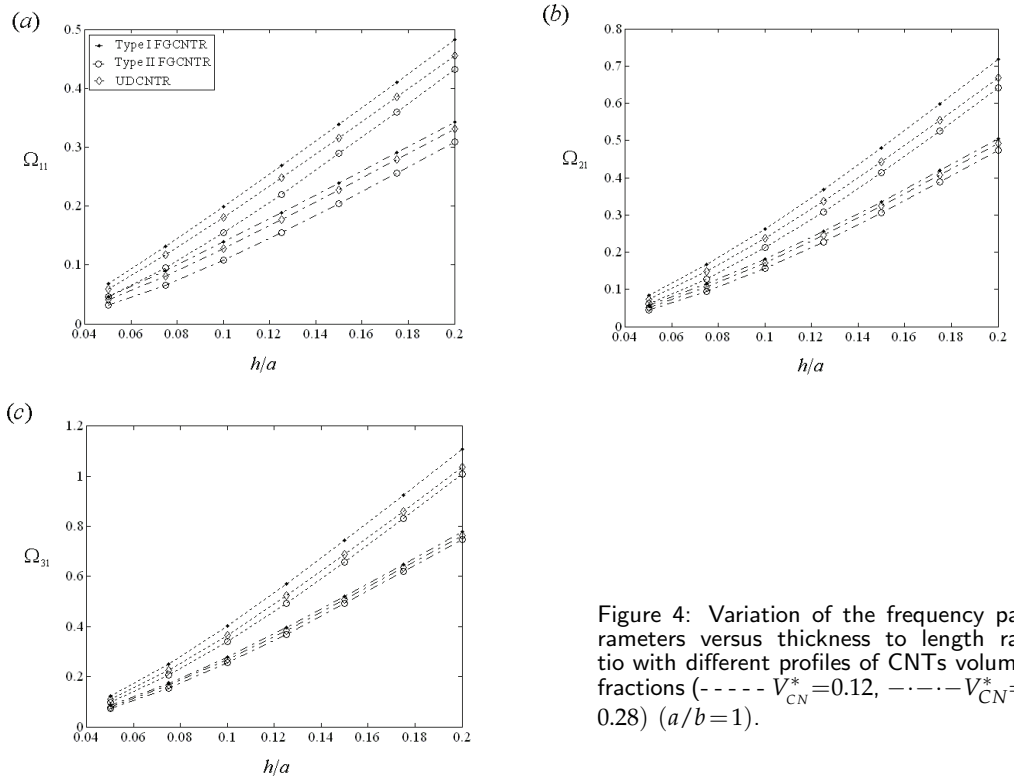

Figure 4: Variation of the frequency parameters versus thickness to length ratio with different profiles of CNTs volume fractions (- - - - - V^*_{CN}=0.12, —·—·— V^*_{CN}= 0.28) $(a/b=1)$.

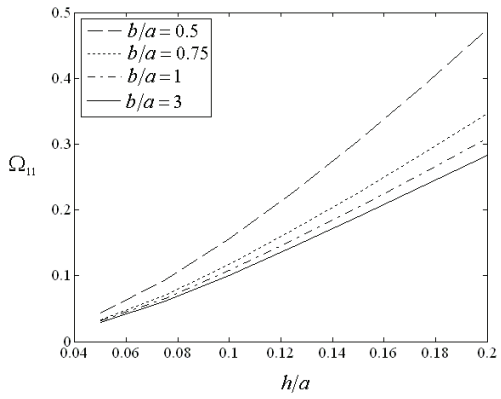

Figure 5: Effect of thickness to length on the fundamental frequency parameter of the FGCNTR plate for different values of b/a ratio $(V^*_{CN}=0.12)$.

UDCNRT frequency parameter ratio is more significant than that of the Type I FGCNRT to UDCNRT frequency parameter ratio. Also it is seen that the discrepancies between the frequency parameters of the Type I FGCNRT and UDCNTR are lower than those of Type II FGCNRT and UDCNTR.

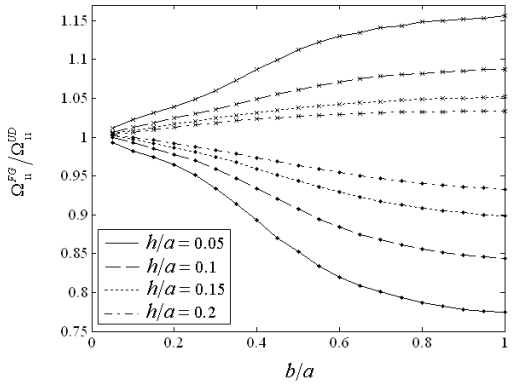

Figure 6: Variation of the $\Omega_{11}^{FG}/\Omega_{11}^{UD}$ ratio versus width to length ratio with for various h/a ratio ($-\times-$ Type I FGCNTR to UDCNTR frequency parameter ratio, $-\diamond-$ Type II FGCNTR to UDCNTR frequency parameter ratio).

4.2.3 Influence of wave number n on frequency parameters

Fig. 7 shows the variation of the Type I FGCNTR to UDCNTR frequency parameter ratio with wave number n for different values of h/a ratio. It can be seen that Type I FGCNTR to UDCNTR frequency parameter ratio decreases rapidly as the wave number n and h/a ratio increases. The influence of CNTs volume fraction on the frequency parameter of the Type II FGCNTR plate for various wave number n and b/a ratio is shown in Fig. 8. From this figure it is apparent that the effect of the CNTs volume fraction is more prominent at high wave number n. In Fig. 9, the variation of the Type II FGCNTR to UDCNTR frequency parameter ratio with wave number n for various b/a ratios is shown. It is worthwhile to mention that with decrease in the b/a ratio, frequency parameter of the FGCNTR plates are very close to those of UDCNTR plates.

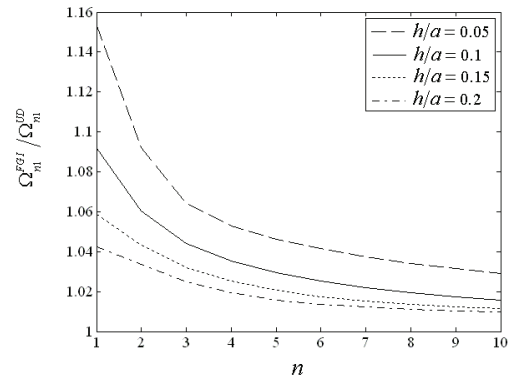

Figure 7: Variation of the Type I FGCNTR to UDCNTR frequency parameter ratio with wave number n for different values of h/a ratio $(b/a = 0.75)$.

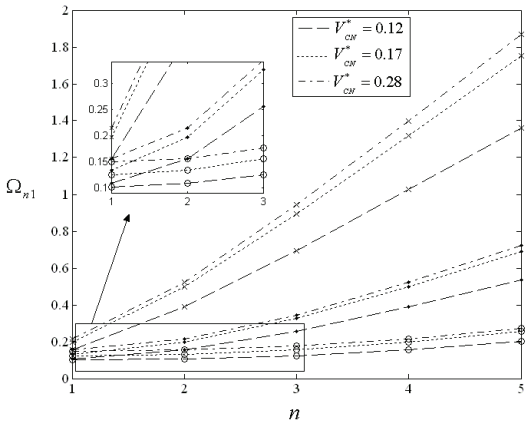

Figure 8: Influence of CNTs volume fraction on the frequency parameter of the Type II FGCNTR plate for various wave number n ($-\times-$ $b/a=0.5$, $-\diamond-$ $b/a=1$, $-\circ-$ $b/a=2$).

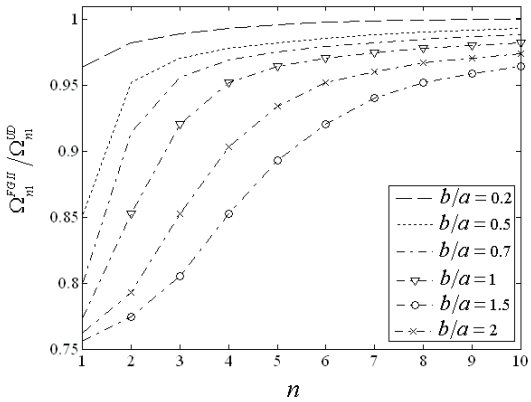

Figure 9: The Type II FGCNTR to UDCNTR frequency parameter ratio of the CNTR plate for different values of b/a ratio and wave number n $(h/a=0.05)$.

4.2.4 Effect of the CNTs volume fraction on frequency parameter

The effect of the CNTs volume fraction V^*_{CN} on the frequency parameter of the FGCNTR plate for various b/a ratio is shown in Fig. 10. It is found that the frequency parameter of the FGCNTR plate is increased with increase in CNTs volume fraction. It should be noted that the frequency parameter decreases rapidly with the increase of the b/a ratio and then remains almost unaltered for $b/a>0.5$. The effect of b/a ratio on the fundamental frequency parameter of the Type I FGCNTR plate for various CNTs volume fraction is presented in Fig. 11. It can be concluded that the influence of the CNTs volume fraction on the fundamental frequency parameter of the Type I FGCNTR plate is generally significant at low b/a ratio.

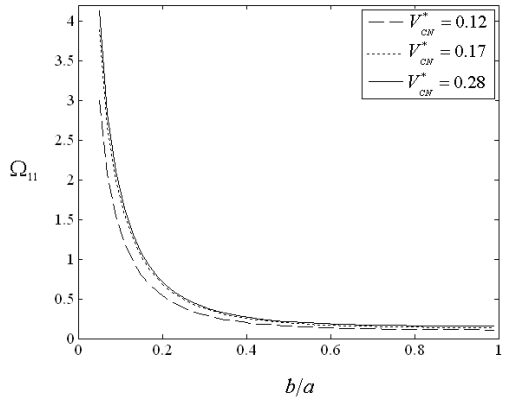

Figure 10: Effect of CNTs volume fraction on the frequency parameter of the FGCNTR plate for various b/a ratio $(h/a=0.1)$.

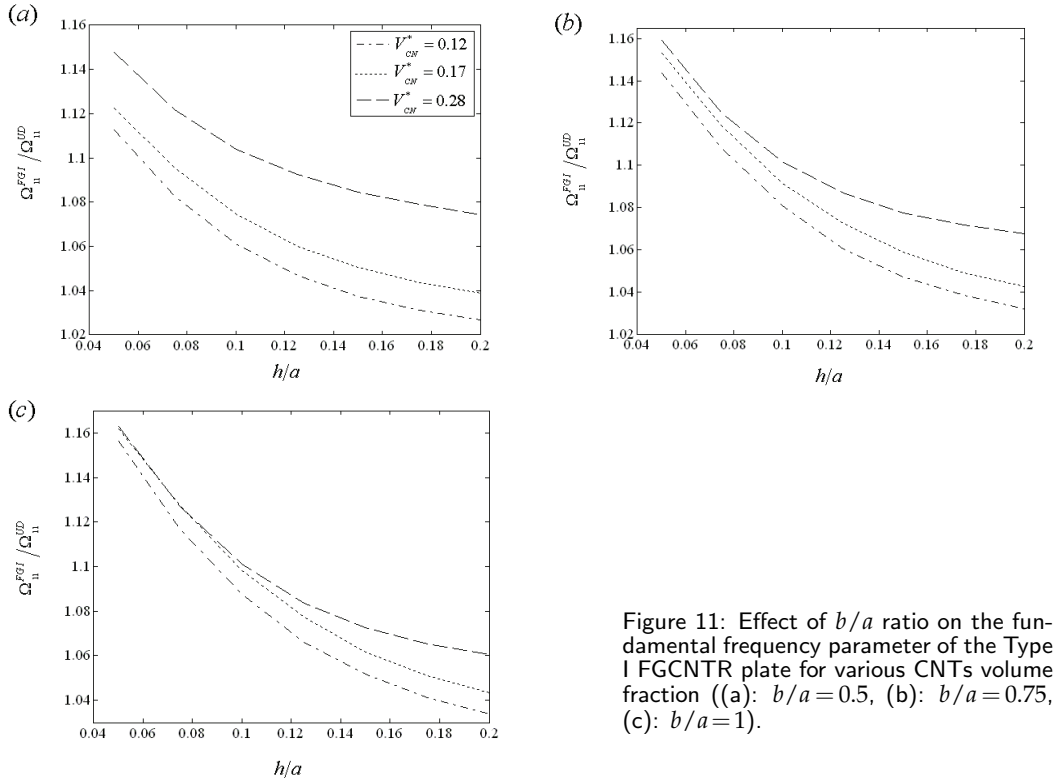

Figure 11: Effect of b/a ratio on the fundamental frequency parameter of the Type I FGCNTR plate for various CNTs volume fraction ((a): $b/a=0.5$, (b): $b/a=0.75$, (c): $b/a=1$).

4.2.5 Impact of prediction models of material properties on frequency parameter

In order to investigate the prediction methods of the mechanical properties of nanocomposites, the frequency parameters obtained from extended rule of mixture are compared

Table 3: Non-dimensional natural frequency parameters of nanocomposite square plate with prediction methods of the mechanical properties of nanocomposites.

		Extended rule of mixture			Eshelby-Mori-Tanaka approach		
V_{CN}^*	h/a	Type I	UD	Type II	Type I	UD	Type II
0.12							
	0.01	0.002168	0.001797	0.001321	0.002157	0.001770	0.001304
	0.05	0.046574	0.040326	0.031155	0.046316	0.040160	0.030945
	0.1	0.138998	0.127824	0.107776	0.138154	0.124965	0.106101
	0.15	0.239550	0.227818	0.204612	0.237812	0.224701	0.202019
	0.2	0.342507	0.331268	0.309019	0.340802	0.330018	0.307549
0.17							
	0.01	0.002536	0.002095	0.001526	0.002522	0.002073	0.001507
	0.05	0.052363	0.045605	0.035409	0.052259	0.045468	0.035198
	0.1	0.149456	0.138447	0.118676	0.147904	0.136195	0.115931
	0.15	0.252229	0.240654	0.219649	0.250821	0.389605	0.218164
	0.2	0.357232	0.345423	0.326300	0.355096	0.342901	0.325134
0.28							
	0.01	0.003179	0.002616	0.001890	0.003155	0.002601	0.001838
	0.05	0.062227	0.05432	0.042818	0.062079	0.054134	0.042256
	0.1	0.168995	0.155834	0.137657	0.166601	0.153361	0.133259
	0.15	0.279679	0.263376	0.247275	0.277491	0.261496	0.243801
	0.2	0.393079	0.373005	0.360713	0.391132	0.369814	0.358924

in Tables 3 and 4 with those of Eshelby-Mori-Tanaka method for various types of CNT volume fraction profiles and different values of h/a and b/a ratio. It can be concluded from Tables 3 and 4 that prediction methods of effective material properties have an insignificant influence of the variation of the frequency parameters with h/a and b/a ratio. It should be noted that the extended rule of mixture has higher frequency parameter than that of the Eshelby-Mori-Tanaka approach.

5 Conclusion remarks

Based on the first-order shear deformation theory (FSDT) and generalized differential quadrature (GDQ), a comprehensive study of the free vibration analysis of the simply supported functionally graded carbon nanotube-reinforced (FGCNTR) plates was investigated. The FGCNTR plate was assumed to be made from a mixture of aligned and straight SWCNT, graded distribution in the thickness direction, and matrix which was assumed to be isotropic. The material properties of SWCNT were determined according to molecular dynamics (MD) and then the effective material properties of CNTRCs were estimated through the rule of mixture in which the CNT efficiency parameters were introduced to account for the scale-dependence of the resulting nanostructures. Further-

Table 4: Comparison of the natural frequency parameters obtained by extended rule of mixture and Eshelby-Mori-Tanaka method for different values of b/a ratio $(h/a=0.05)$.

$h/a=0.05$		Extended rule of mixture			Eshelby-Mori-Tanaka approach		
V^*_{CN}	b/a	Type I	UD	Type II	Type I	UD	Type II
0.12							
	0.2	0.182781	0.176030	0.169707	0.180258	0.173855	0.167720
	0.5	0.057302	0.051543	0.043897	0.057124	0.051268	0.043675
	1	0.046574	0.040326	0.031155	0.046349	0.040109	0.031019
	1.5	0.045553	0.039246	0.029877	0.045285	0.039035	0.029482
	2	0.045286	0.038964	0.029545	0.044994	0.038799	0.029350
0.17							
	0.2	0.191026	0.180989	0.172456	0.189501	0.178558	0.171105
	0.5	0.062688	0.056063	0.047136	0.062352	0.055799	0.045990
	1	0.052363	0.045605	0.035409	0.052174	0.045375	0.035291
	1.5	0.051426	0.044644	0.034290	0.051224	0.044415	0.034134
	2	0.051187	0.044398	0.034004	0.051008	0.044260	0.033862
0.28							
	0.2	0.214772	0.193184	0.179656	0.213001	0.191950	0.178509
	0.5	0.073081	0.064184	0.053337	0.072916	0.064073	0.053183
	1	0.062227	0.054321	0.042818	0.062095	0.054150	0.042566
	1.5	0.061298	0.053466	0.041873	0.061128	0.053209	0.041644
	2	0.061069	0.053254	0.041636	0.060793	0.053076	0.040061

more, the material properties of SWCNT can be used to calculate the elastic properties of nanocomposites using the Mori-Tanaka modified approach that utilizes Eshelby tensors. The following conclusions can be drawn from the present:

- The achieved results show that the FGCNTR plates with symmetric profiles of the CNTs volume fraction can likely be designed according to the actual requirement and it is a potential alternative to the CNTRc plates with uniformly distributed CNTs.

- Results indicate the prediction methods (extended rule of mixture and Eshelby-Mori-Tanaka method) of effective material properties have an insignificant influence of the variation of the frequency parameters with h/a and b/a ratio.

- The extended rule of mixture has higher frequency parameter than that of the Eshelby-Mori-Tanaka method.

- It is observed that the effect of the h/a ratio on the Type II FGCNRT to UDCNRT frequency parameter ratio is more significant than that of the Type I FGCNRT to UDCNRT frequency parameter ratio.

References

[1] E. T. THOSTENSON, Z. REN AND T. W. CHOU, *Advances in the science and technology of carbon nanotubes and their composites: a review*, Compos. Sci. Tech., 61 (2001), pp. 1899–1912.

[2] S. STANKOVICH, D. A. DIKIN, G. H. B. DOMMETT, K. M. KOHLHAAS, E. J. ZIMNEY AND E. A. STACH ET AL., *Graphene-based composite materials*, Nature, 442 (2006), pp. 282–286.

[3] T. RAMANATHAN, A. A. ABDALA, S. STANKOVICH, D. A. DIKIN, M. HERRERA-ALONSO AND R. D. PINER ET AL., *Functionalized graphene sheets for polymer nanocomposites*, Nat. Nanotech., 3 (2008), pp. 327–331.

[4] D. QIAN, G. J. WAGNER, W. K. LIU, M. F. YU AND R. S. RUOFF, *Mechanics of carbon nanotubes*, Appl. Mech. Rev., 55 (2002), 495.

[5] R. B SEYMOUR, Polymeric Composites, VSP, the Netherlands, 1990.

[6] P. MORGAN, Carbon Fibers and their Composites, CRC Press, Taylor and Francis Group, 2005.

[7] J. A. H. HUIT AND K. G. RAMMERSTORFER, Engineering Mechanics of Fiber Reinforced Polymers and Composite Structures, Springer Verlag, 1994.

[8] E. FITZER AND L. M. MANOCHA, Carbon Reinforcements and Carbon/Carbon Composites, Springer-Verlag, 1998.

[9] E. T. THOSTENSON, Z. F. REN AND T. W. CHOU, *Advances in the science and technology of carbon nanotubes and their composites: a review*, Compos. Sci. Tech., 61(13) (2001), pp. 1899–1912.

[10] M. MONIRUZZAMAN AND K. I. WINEY, *Polymer nanocomposites containing carbon nanotubes*, Macromolecules, 39 (2006), pp. 5194–5205.

[11] V. BAVASTRELLO, M. K. RAM AND C. NICOLINI, *Synthesis of multiwalled carbon nanotubes and poly(o-anisidine) nanocomposite material: fabrication and characterization of its Langmuir-Schaefer films*, Langmuir., 18 (2002), pp. 1535–1541.

[12] D. QIAN, E. C. DICKEY, R. ANDREWS AND T. RANTELL, *Load transfer and deformation mechanisms in carbon nanotube-polystyrene composites*, Appl. Phys. Lett., 76 (2000), pp. 2868–2670.

[13] H. S. SHEN, *Nonlinear bending of functionally graded carbon nanotube-reinforced composite plates in thermal environments*, Compos. Struct., 91 (2009), pp. 9–19.

[14] Z. X. WANG AND H. S. SHEN, *Nonlinear vibration and bending of sandwich plates with nanotube-reinforced composite face sheets*, Compos. Part B Eng., Article in Press, 2011, doi:10.1016/j.compositesb.2011.04.040.

[15] H. S. SHEN AND Z. H. ZHU, *Buckling and postbuckling behavior of functionally graded nanotube-reinforced composite plates in thermal environments*, Comput. Mater. Continua., 18 (2010), pp. 155–182.

[16] H. S. SHEN AND C. L. ZHANG, *Thermal buckling and postbuckling behavior of functionally graded carbon nanotube-reinforced composite plates*, J. Mater. Design, 31 (2010), pp. 3403–3411.

[17] L. L. KE, J. YANG AND S. KITIPORNCHAI, *Nonlinear free vibration of functionally graded carbon nanotube-reinforced composite beams*, Compos. Struct., 92 (2010), pp. 676–683.

[18] M. H. YAS AND M. HESHMATI, *Dynamic analysis of functionally graded nanocomposite beams reinforced by randomly oriented carbon nanotube under the action of moving load*, Appl. Math. Model., 36 (2012), pp. 1371–1394.

[19] R. MORADI-DASTJERDI, M. FOROUTAN AND A. POURASGHAR, *Dynamic analysis of functionally graded nanocomposite cylinders reinforced by carbon nanotube by a mesh-free method*, J. Mater. Design, 44 (2013), pp. 256–266.

[20] A. ALIBEIGLOO, *Static analysis of functionally graded carbon nanotube-reinforced compos-*

ite plate embedded in piezoelectric layers by using theory of elasticity, Compos. Struct., http://dx.doi.org/10.1016/j.compstruct.2012.08.018.

[21] G. M. ODEGARD, T. S. GATES, K. E. WISE, C. PARK AND E. J. SIOCHI, *Constitutive modeling of nanotubereinforced polymer composites*, Compos. Sci. Tech., 63 (2003), pp. 1671–1687.

[22] Y. BENVENISTE, *A new approach to the application of Mori-Tanaka's theory in composite materials*, Mech. Mater., 6 (1987), pp. 147–157.

[23] C. H. CHEN, *Effective elastic moduli of misoriented short-fiber composites*, Int. J. Solids Struct., 33 (1996), pp. 2519–2539.

[24] E. SHADY AND Y. GOWAYED, *Effect of nanotube geometry on the elastic properties of nanocomposites*, Compos. Sci. Tech., 70 (2010), pp. 1476–1481.

[25] J. D. ESHELBY, *The determination of the elastic field of an ellipsoidal inclusion and related problems*, Proc. Royal Society London, Series A, 241 (1957), pp. 376–396.

[26] J. D. ESHELBY, *The elastic field outside an ellipsoidal inclusion*, Proc. Royal Soc. A, 252 (1959), pp. 561–569.

[27] S. GIORDANO, P. L. PALLA AND L. COLOMBO, *Nonlinear elasticity of composite materials Landau coefficients in dispersions of spherical and cylindrical inclusions*, Euro. Phys. J. B, 68 (2009), pp. 89–101.

[28] T. MORI AND K. TANAKA, *Average stress in matrix and average elastic energy of materials with misfit ting inclusions*, Acta. Metall, 21 (1973), pp. 571–574.

[29] G. FORMICA, W. LACARBONARA AND R. ALESSI, *Vibrations of carbon nanotube-reinforced composites*, J. Sound Vib., 329 (2010), pp. 1875–1889.

[30] D. L. SHI, X. Q. FENG, Y. Y. HUANG, K. C. HWANG AND H. GAO, *The effect of nanotube waviness and agglomeration on the elastic property of carbon nanotube-reinforced composites*, J. Eng. Mater Tech., 126 (2004), pp. 250–257.

[31] T. MURA, Micromechanics of Defects in Solids, The Hague: Martinus Nijhoff; 1982.

[32] R. HILL, *A self-consistent mechanics of composite materials*, J. Mech. Phys. Solids, 13 (1965), pp. 213–222.

[33] R. D. MINDLIN, *Influence of rotatory inertia and shear on flexural motions of isotropic elastic plates*, American Society of Mechanical Engineers, J. Appl. Mech., 18 (1951), pp. 31–38.

[34] F. NORMAN, J. R. KNIGHT AND Q. YUNQIAN, *On a consistent first-order shear-deformation theory for laminated plates*, Compos. Part B, 28(4) (1977), pp. 397–405.

[35] M. E. FARES, *Non-linear bending analysis of composite laminated plates using a refined first-order theory*, Compos. Struct., 46(3) (1999), pp. 257–266.

[36] C. SHU, Differential Quadrature and Its Application in Engineering, Springer, Berlin, 2000.

[37] C. SHU AND B. RICHARDS, *Application of generalized differential quadrature to solve two-dimensional incompressible Navier Stockes equations*, Int. J. Numer Meth. Fl., 15 (1992), pp. 791–798.

[38] C. SHU, *Free vibration analysis of composite laminated conical shells by generalized differential quadrature*, J. Sound Vib., 194 (1996), pp. 587–604.

[39] J. N. REDDY, Theory and Analysis of Elastic Plates, Taylor and Francis, Philadelphia, 1999.

[40] M. H. YAS AND B. SOBHANI ARAGH, *Free vibration analysis of continuous grading fiber reinforced plates on elastic foundation*, Int. J. Eng. Sci., 48 (2010), pp. 1881–1895.

[41] H. MATSUNAGA, *Free vibration and stability of functionally graded plates according to a 2D higher-order deformation theory*, J. Compos. Struct., 82 (2008), pp. 499–512.

[42] Y. HAN AND J. ELLIOTT, *Molecular dynamics simulations of the elastic properties of polymer/carbon nanotube composites*, Comput. Mater. Sci., 39 (2007), pp. 315–323.